PHYSICAL REVIEW A VOLUME 57, NUMBER 6 JUNE 1998

Quasiclassical study of differential inelastic scattering of oriented Ca$(4s5p,{}^1P_1)$ atoms on He

A. Devdariani and E. Tchesnokov
Department of Physics, St. Petersburg University, St. Petersburg 199034, Russia

E. I. Dashevskaya and E. E. Nikitin
Department of Chemistry, Technion, Haifa 32000, Israel

(Received 15 December 1997)

A quasiclassical analysis of the differential inelastic scattering of oriented Ca$(4s5p,{}^1P_1)$ atoms on He at a collision energy of 1 eV is presented. Inelastic channels correspond to spin-changing events populating different Zeeman sublevels of three fine-structure states of Ca$(4s5p,{}^3P_j)$, $j=0$, 1, and 2. The magnitude of the right-left scattering asymmetry in the helicopter plane is shown to depend on the locking dynamics. The relative values of different Zeeman-specific cross sections are determined by the diffraction scattering on the attractive ${}^1\Pi$ state in the entrance channels, by the Coriolis mixing between degenerate components of the repulsive ${}^3\Sigma^+$ intermediate state, and by the radial coupling between 1-1 and 0^--0^- fine-structure components of the ${}^3\Sigma^+$-${}^3\Pi_\Omega$ states in the exit channels. The predicted large right-left scattering asymmetry suggests that it can be measured experimentally. [S1050-2947(98)07106-6]

PACS number(s): 34.50.−s

I. INTRODUCTION

Recently, quasiclassical calculations of differential cross sections for Na*-Ne [1,2] and Ne*-Ar [3] scattering at low energies within the so-called sudden locking approximation were carried out. For the former system, it was found that this approximation reproduces well the accurate close-coupling quantal results [4], and also helps to understand the oscillatory interference structure of the cross section for the scattering of unpolarized sodium atoms in either of its fine-structure states ${}^2P_j$, $j=\frac{1}{2}$ and $\frac{3}{2}$ [5]. For the latter system, the quasiclassical locking approximation qualitatively explains the experimentally detected right-left azimuthal asymmetry in the scattering of helicopter-polarized atoms Ne*$(2p^53s,{}^3P_2)$ [6]. In both cases, the locking approximation was applied under the conditions that the initial and final states belong to the same (or virtually the same) energy level of colliding species, and that in the molecular region there is no coupling between different molecular states. Since the quasiclassical locking approximation showed itself to be quite helpful in the above cases, we thought that its application to more complicated events would be of interest. We have chosen the spin-changing collisions of calcium as an example of such a system;

$$\mathrm{Ca}^*(4s5p,{}^1P_1)+\mathrm{He}\rightarrow\mathrm{Ca}^*(4s5p,{}^3P_j)+\mathrm{He}. \qquad (1)$$

For this collision event, the molecular states features different types of coupling which can be treated analytically in terms of Landau-Zener, Demkov, and Nikitin models.

Recent theoretical studies of this process were motivated by cell experiments on spin-changing collisions ${}^1P\rightarrow{}^3P$ [7], as well as an intramultiplet mixing between ${}^3P_j$ multiplet levels [7,8] and especially on the alignment effect in molecular beam studies [9,10]. Related studies include measurements of the absorption profile of the Ca$(4s^2,{}^1S-4s5p,{}^1P)$–He transitions, and the dependence of the spin-changing transitions in the far-wing laser scattering [11,12] on the detuning.

The existing theoretical studies of Ca-He collisions fall into three different categories. The first is based on a semiclassical treatment of the dynamical problem [13,14]. The adiabatic potential curves were calculated from the effective Hamiltonian approach, as described in Ref. [15], supplemented with the multiple-scattering method for a description of the short-range part of the interaction of the excited electron of Ca with He [16]. In Ref. [17], a generalization of this method for many-election outer shells and the intermediate angular momenta coupling case was suggested. Within this approach, crossing between molecular potentials ${}^3\Sigma^+$ [correlating with ${}^3P_2(\mathrm{Ca})+{}^1S_0(\mathrm{He})$] and ${}^1\Pi$ [correlating with ${}^1P_1(\mathrm{Ca})+{}^1S_0(\mathrm{He})$] was predicted, and the crossing distance R_0 was estimated as 15 a.u. This permitted the authors of Ref. [14] to obtain a reasonable agreement with experimental data [7,9]. Additional intersections and extrema for $R<R_0$ were predicted in Refs. [18,19], and configuration interaction effects have been incorporated [20] into calculations of adiabatic potential curves. The latter refinement led to quite good agreement with experimental data on spectral line satellites [11].

The second approach, as described in Refs. [21–25], is based on close-coupling calculations using the model potential calculations of similar systems [22] and flexible Morse-spline van der Waals forms. The choice of parameters in the potentials was guided by the desire to reproduce the experimental results as reported in Refs. [7,9]. Although the agreement for the spin-changing reaction and intramultiplet mixing and alignment effects [9] are rather good, an intersection distance R_0 of about 8.5 a.u. seems to be too small, as one can judge from later calculations (see below); moreover, the potential curves adopted did not show additional intersections and extrema. This approach was also used for a calculation of the total cross section for different final Zeeman states of the Ca atom [26]. The particular choice of the initial

1050-2947/98/57(6)/4472(11)/$15.00

© 1998 The American Physical Society

states was guided by the experimental conditions [27].

The third approach concentrated solely on a calculation of the potential curves. The theoretical method was based on l-dependent pseudopotentials. The first calculations along this line [28] yielded a value of R_0 of about 13 a.u., and provided an independent confirmation of the existence of additional extrema at smaller R_0. The improved version of this approach [29] gave a value of R_0 of about 16 a.u. However, a comparison with experimental data on the satellites of Ca$(4s^2,{}^1S-4s5p,{}^1P)$–He optical transitions [11] led to the conclusion that the theory seemed to overestimate the repulsion at small R. The latter conclusion can also be drawn from the comparison of the theoretical and experimental data on far-wing profiles for another system, Li$(2p-3d)$-He [30], for which the potential curves were calculated by a similar method.

Neither of the above theoretical works provided a complete set of Zeeman-specific differential cross sections in a spin-changing collision [Eq. (1)]. In the present paper we address this problem using the potential curves from Ref. [19], and a simplified semiclassical description that adopts the locking approximation. The use of this approximation makes it easy to establish a correlation between general features of the differential cross sections and the pattern of adiabatic potential curves. The results obtained can be regarded as approximate theoretical predications for anticipated experiments.

The plan of the presentation is the following. In Sec. II, we discuss the molecular potential curves of the Ca*He system, and identify the range of interatomic distances important for the dynamics of reaction (1). In Sec. III the general quasiclassical approximation to the scattering amplitudes is presented. Sections IV and V deal with the locking matrices and the molecular scattering matrices. The differential and integral cross sections are calculated in Sec. VI. Finally, Sec. VII summarizes our findings.

II. ADIABATIC POTENTIALS OF Ca$(4s5p)$–He QUASIMOLECULE

The adiabatic potential curves used in this paper were borrowed from our earlier calculations [18,19], and correspond to the eigenvalues of the electronic Hamiltonian. The matrix of this Hamiltonian was built on the basis of one-electron wave functions of the excited Ca atom, on the spin-orbit interaction in a free Ca atom, and also on the exchange and polarization interaction between Ca* and He. These potentials are shown in Fig. 1. They are completely determined by the following parameters: the singlet-triplet spacing ΔE in free Ca atom (expressed via the Slater exchange integral); the fine-structure splittings $\Delta\varepsilon_{20}$ and $\Delta\varepsilon_{21}$ in free-atom Ca; and two R-dependent matrix elements V_Σ and V_Π, that describe the interaction between a hypothetical atom Ca*, possessing no spin-orbit coupling, and atom He.

An interesting feature of these potential curves are the maxima for ${}^3\Sigma^+$ and ${}^1\Sigma^+$ states at about $R=10$ a.u. These maxima are related to the maximum of the radial wave function of the excited electron of Ca, which explains why two Σ curves run almost parallel to each other. The maximum of the same origin exists for a simpler system K*-He, where instead of two Σ curves there exists one doublet Σ curve which passes through its maximum at about 13 a.u. [31]. We attribute the difference in the position of the maximum for Ca*-He and K*-He systems to a more compact shape of the wave functions of a $5p$ electron in Ca. We also note that the Σ curves without maxima, proposed in Ref. [24] and used later for quantum flux studies in the Ca*-He system [32], were modified in Ref. [33] in such a way as to produce maxima.

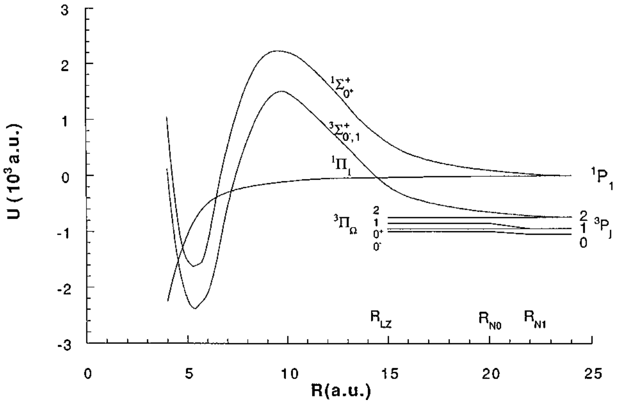

FIG. 1. Adiabatic potential curves for the system Ca*-He.

We believe that theoretical calculations of potential curves at interatomic distances $R<5$ a.u., that correspond to the repulsion, are not reliable, since the applicability conditions of the method used in Ref. [16] are marginally fulfilled. For a collision energy of 1 eV, this part of the potential is essential for scattering through angles larger than 0.25 rad. At these angles, the cross sections are very small, and they were not considered in this paper. Therefore these portions of the curves are not shown in Fig. 1. On the other hand, part of the potentials just to the left of the barrier maxima are important for the differential cross sections for the scattering through the angles discussed in this paper.

III. SCATTERING AMPLITUDES

We will use a quasiclassical approximation for the scattering amplitudes in the space-fixed (SF) center-of-mass frame xyz. The x axis of this frame is directed opposite to the initial wave vector of relative motion $\mathbf{k}$, and the z axis is chosen to be an appropriate quantization axis for the electronic angular momentum of free Ca atom. Let ajn and $a'j'n'$ be the initial and final electronic quantum numbers of Ca (a and a' stand for the Russell-Sounders nomenclature ${}^1P$ and ${}^3P$; j' and j are the electronic angular momenta, and n' and n are their projections onto the z axis). The scattering amplitude in this frame, $F^{xyz}_{a'j'n';ajn}(\theta,\varphi)$, depends on two angles; the polar angle θ of the final wave vector $\mathbf{k}'$ with respect to $\mathbf{k}$, and the azimuthal angle φ which is counted from the y axis in the yz plane. Along with the SF frame, we consider the natural collision frame (NCF) XYZ [1]. The X axis of this frame coincides with x axis of the SF frame, and the Z axis is parallel to the vector product of the final and initial wave vectors, $\mathbf{k}'\times\mathbf{k}$. Clearly, the Y axis of NCF makes the angle φ with y axis. The scattering amplitude in the NCF is independent of φ; let it be $F^{XYZ}_{a'j'n';ajn}(\theta)$. Two amplitudes, F^{xyz} and F^{XYZ} are trivially related to each other by rotation about the x (or X) axis, and by reflection in the

XY plane [15]. We will consider particular cases of this transformation that corresponds to the right and left scattering in the SF frame.

The scattering to the right through angle θ is defined by the value of the azimuthal angle $\varphi=0$, while the scattering to the left corresponds to $\varphi=\pi$. We just have [1]

$$F^{xyz,\mathrm{right}}_{a'j'n';ajn}(\theta)\equiv F^{xyz}_{a'j'n';ajn}(\theta,\varphi=0)=F^{XYZ}_{a'j'n';ajn}(\theta),$$

$$F^{xyz,\mathrm{left}}_{a'j'n';ajn}(\theta)\equiv F^{xyz}_{a'j'n';ajn}(\theta,\varphi=\pi) =(-1)^{j'-j}F^{XYZ}_{a'j'-n';aj-n}(\theta). \tag{2}$$

We see that the left-right azimuthal asymmetry in the SF frame is described by NCF amplitudes with opposite projections of electronic angular momentum onto the Z axis. Note also that for the forward scattering ($\theta=0$) the amplitudes, $F^{xyz,\mathrm{right}}_{a'j'0;aj0}(0)$ and $F^{xyz,\mathrm{left}}_{a'j'0;aj0}(0)$ should be equal to each other; on the other hand, Eq. (2) implies that if $|j'-j|$ is odd, they differ in sign. Therefore we have $F^{XYZ}_{a'j'0;aj0}(0)=0$, provided $|j'-j|$ is odd. In what follows we will discuss only the NCF amplitudes, and for simplicity drop the superscript XYZ.

The quasiclassical approximations for NCF amplitudes falls into two categories: one corresponds to the scattering through classical angles, $\theta\gg\theta_{\mathrm{diff}}$ (θ_{diff} being the diffraction angle), and the other to the scattering through small angles, $\theta\ll 1$, which also includes nonclassical (diffraction) angles, $\theta\leq\theta_{\mathrm{diff}}$. Since under quasiclassical conditions θ_{diff} is very small ($\theta_{\mathrm{diff}}\approx 1/kR_0$, where R_0 is a range of the potential), these two cases possess the common region of applicability, $\theta_{\mathrm{diff}}\ll\theta\ll 1$.

For scattering through classical angles, the amplitude $F_{a'j'n';ajn}(\theta)$ can be written via two auxiliary functions $f^{+}_{a'j'\nu';aj\nu}(\theta)$ and $f^{-}_{a'j'\nu';aj\nu}(\theta)$, which in turn are expressed via the scattering matrix in the J-helicity body-fixed representation $S_{a'j'\nu';aj\nu}(J)$ (ν and ν' are projections of $\mathbf{j}$ and $\mathbf{j}'$ onto the classical total angular momentum vector $\mathbf{J}$) [1]:

$$F_{a'j'n';ajn}(\theta)=\exp[in'(\theta-\pi)][f^{+}_{a'j'\nu';aj\nu}(\theta)|_{\substack{\nu'=n'\\ \nu=n}} +(-1)^{j'+j}f^{-}_{a'j'\nu';aj\nu}(\theta)|_{\substack{\nu'=-n'\\ \nu=-n}}], \tag{3}$$

$$f^{+}_{a'j'\nu';aj\nu}(\theta)=\frac{\exp(-i\pi/4)}{\sqrt{2\pi k'k\sin\theta}}\int_0^\infty \exp(-i\theta J) \times S_{a'j'\nu';aj\nu}(J)\sqrt{J}dJ, \tag{4}$$

$$f^{-}_{a'j'\nu';aj\nu}(\theta)=\frac{-\exp(i\pi/4)}{\sqrt{2\pi k'k\sin\theta}} \times\int_0^\infty \exp(i\theta J)S_{a'j'\nu';aj\nu}(J)\sqrt{J}dJ. \tag{5}$$

For the scattering through small angles, $F_{a'j'n';ajn}(\theta)$ is represented as

$$F_{a'j'n';ajn}(\theta)=\frac{-i}{\sqrt{k'k}}\int_0^\infty J\,dJ\sum_{m'm\nu'\nu} i^{m-m'} \times J_{m'-m}(\theta J)\Delta^{j'}_{m'n'}\Delta^{j'}_{m'\nu'} \times\exp(-i\pi\nu')S_{a'j'\nu';aj\nu}\Delta^{j}_{mn}\Delta^{j}_{m\nu}, \tag{6}$$

where $J_{m'-m}$ is the Bessel function of order $m'-m$, and $\Delta^{j}_{m\nu}$ are the particular values of the Wigner D functions, $\Delta^{j}_{m\nu}=D^{j}_{mv}(0,\pi/2,0)$; see Ref. [34].

Expressions (3) and (6) become identical to each other when $n'\theta$ is neglected in the exponent of the first factor on the right-hand side of Eq. (3) (scattering angles are small, $\theta\ll 1$), and when the Bessel function on the right-hand side of Eq. (6) is replaced by its asymptotic expression (scattering angles are larger than the diffraction angle, $J\theta\gg 1$). A series of transformations ''initial SF frame–natural collision frame–body-fixed J-helicity frame'' is intended to express the scattering amplitudes through the J-helicity S matrix which has a simple structure, and can be constructed in the so-called locking approximation [1]

$$\mathbf{S}=\mathbf{C}^{\mathrm{Tr}}\mathbf{S}^{M}\mathbf{C}, \tag{7}$$

where $\mathbf{C}$ is the locking matrix, and $\mathbf{S}^{M}$ is the molecular scattering matrix [1]. When rewriting this equation in terms of the matrix elements, we take into account that C matrix is diagonal in aj (these quantum numbers are written as superscripts), and explicitly introduce the reflection symmetry quantum number σ:

$$S^{(\sigma)}_{a'j'\nu';aj\nu}(J)=\sum_{\omega',\omega}C^{a'j'\sigma}_{\omega';\nu'}(J)S^{M,\sigma}_{a'j'\omega';aj\omega}(J)C^{aj\sigma}_{\omega;\nu}(J). \tag{8}$$

Here ω is the absolute value of the R-helicity projection of $\mathbf{j}$, and aj quantum numbers still have a significance in a sense of adiabatic correlation (see Fig. 1). Thus, for process (1), we have the following identification of aj and $a'j'$:

$aj=a1\equiv{}^1P_1$ when it appears in $\mathbf{C}$,

$aj\equiv{}^1\Pi$ when it appears in $\mathbf{S}^M$,

$a'j'\equiv{}^3\Sigma^+,{}^3\Pi$ when it appears in $\mathbf{S}^M$

$a'j'=a'0,a'1,a'2\equiv{}^3P_j(j=0,1,2)$

when it appears in $\mathbf{C}^{\mathrm{Tr}}$.

Note that the scattering matrix decomposes into two blocks that correspond to the positive ($\sigma=1$) and negative ($\sigma=-1$) reflection symmetries. Actually, the quantum number σ on the left-hand side of Eq. (8) is redundant (hence it is bracketed), since σ is related to the J-helicity quantum number ν and the parity of the state w as $\sigma=w(-1)^{\nu}$ [the parity quantum number implicitly enters into the set a; for collision (1) $w=w'=-1$].

In our case, with the initial $4s5p,{}^1P_1$ state, the positive substates are $j=1$ and $\nu=\pm 1$, and the negative substates are $j=1$ and $\nu=0$. The final states $4s5p.\ {}^3P_j$ include both positive and negative substates: the former are $j=1$ and $\nu=\pm 1$ and $j=2$ and $\nu=\pm 1$, while the latter are $j=0,1,2$ and $\nu=0$ and $j=2$ and $\nu=\pm 2$. This yields 13 nonzero elements of the scattering matrix that connect the initial singlet and final triplet states. The number of different cross sections which describe the transfer of state moments in process (1) is larger than the number of nonzero elements of the scattering matrix, since these cross sections are generated from different bilinear combinations of the elements of the scattering matrix. However, if we restrict ourselves to a transition between states of the helicopter polarization (the orientation of j and j' perpendicular to the collision plane), the number of different cross sections, $q_{a'j'n';ajn}(\theta)$, will be equal to the number of nonzero elements of the scattering matrix. Explicitly, the differential cross sections for the scatting to the right and left in the SF frame are

$$\begin{aligned} q^{\text{right}}_{a'j'n';ajn}(\theta) &= |F_{a'j'n';ajn}(\theta)|^2, \\ q^{\text{left}}_{a'j'n';ajn}(\theta) &= |F_{a'j'-n';aj-n}(\theta)|^2, \end{aligned} \tag{9}$$

Out of 13 cross sections, three correspond to $({}^1P_1, j=1,\ n=0) \rightarrow ({}^3P, j=0,1,2,\ n=0)$ right-left invariant transitions, while ten others, $({}^1P_1, j=1,\ n=\pm 1) \rightarrow ({}^3P, j=1,2,\ n=\pm 1, \mp 1)$ and $({}^1P_1, j=1,\ n=0) \rightarrow ({}^3P, j=2,\ n=\pm 2)$, represent five right-left pairs.

IV. LOCKING MATRIX

A locking matrix describes the coupling of the electronic angular momentum $\mathbf{j}$ to the molecular axis as a result of interatomic interaction when two atoms approach each other. In our case this coupling corresponds to the transition from the Hund coupling case e to the coupling case c. Before the collision, the good quantum number of the system is ν, the J-helicity projection of $\mathbf{j}$. After $\mathbf{j}$ is coupled to the molecular axis, the good quantum number is the R-helicity projection of $\mathbf{j}$, or its absolute value ω and the reflection quantum number σ. For the case under consideration, the following blocks of the locking matrix are of interest.

(i) In the entrance channels, the 3×3 locking matrix with elements $C^{a1\sigma}_{\omega;\nu}$ factors out into a 2×2 block $C^{a1+}_{\omega;\nu}$ $(\omega=1,0;\ \nu=1,-1)$, and a single element $C^{a1-}_{1;0}=1$.

(ii) In the exit channels, the 9×9 locking matrix factors out into two diagonal elements $C^{a'0-}_{0;0}=1$, $C^{a'1-}_{1;0}=1'$; two 2×2 blocks with the elements $C^{a'1+}_{\omega;\nu}$ $(\omega=1,0;\ \nu=1,-1)$ and $C^{a'2+}_{\omega;\nu}$ $(\omega=2,1;\ \nu=1,-1)$; and one 3×3 block with the elements $C^{a'2-}_{\omega;\nu}$ $(\omega=2,1,0;\ \nu=2,0,-2)$.

The structure of the 2×2 locking matrix which connects states $|\nu\rangle$ and $|\omega^\sigma\rangle$ is well understood [35,36]. It can be represented in the form

$$\begin{pmatrix} 1^+ \\ 0^+ \end{pmatrix} = (C^{a1+}_{\omega\nu}) \begin{pmatrix} +1 \\ -1 \end{pmatrix},$$

$$(C^{a1+}_{\omega;\nu}) = \begin{pmatrix} \sqrt{1/2+s}\ \exp(i\alpha) & \sqrt{1/2-s}\ \exp(-i\alpha) \\ -\sqrt{1/2-s}\ \exp(i\alpha) & \sqrt{1/2+s}\ \exp(-i\alpha) \end{pmatrix}, \tag{10}$$

where two parameters α and s are the locking angle and the slipping probability. The sudden locking (SL) limit ${}^{\text{SL}}C^{a1+}_{\omega;\nu}$ of the matrix $C^{a1+}_{\omega;\nu}$ corresponds to $s=0$. We have calculated parameters α and s in matrix (10), as suggested in Ref. [36], and found that, for the case under discussion (collision energy 1 eV), both α and s are well represented by the linear functions of the impact parameter b.

The 3×3 locking matrix presumably has no simple representation [37]. Its sudden locking limit for the state $j=2$ is

$$\begin{pmatrix} 2^- \\ 1^- \\ 0^- \end{pmatrix} = ({}^{\text{SL}}C^{a'2-}_{\omega;\nu}) \begin{pmatrix} +2 \\ 0 \\ -2 \end{pmatrix},$$

$$\begin{aligned} &({}^{\text{SL}}C^{a'2-}_{\omega;\nu}) \\ &= \begin{pmatrix} \sqrt{1/8}\ \exp(2i\alpha) & \sqrt{3/4} & \sqrt{1/8}\ \exp(-2i\alpha) \\ -\sqrt{1/2}\ \exp(2i\alpha) & 0 & \sqrt{1/2}\ \exp(-2i\alpha) \\ \sqrt{3/8}\ \exp(2i\alpha) & -\frac{1}{2} & \sqrt{3/8}\ \exp(-2i\alpha) \end{pmatrix}. \end{aligned} \tag{11}$$

We have solved the 3×3 nonsudden locking problem numerically for a range of impact parameters, and found that, with an accuracy of 5% the locking matrix can be represented as

$$\mathbf{C} = \mathbf{M}^{\text{SL}}\mathbf{C}, \quad (M^{a',-}_{\omega',\omega}) = \begin{pmatrix} 1 & 0 & 0 \\ 0 & 1 & -s_{10} \\ 0 & s_{10} & 1 \end{pmatrix}. \tag{12}$$

Here the structure of the correction matrix M has been found from a related study of the 2×2 problem. The values of the parameters α in Eq. (11) and s in Eq. (12) are the same as in Eq. (10), because of the same spacing between the singlet and triplet potential curves.

V. MOLECULAR SCATTERING MATRIX

A molecular scattering matrix describes the fictitious scattering event in which the long-range Coriolis coupling between molecular states is suppressed. As a result, ${}^MS$ possesses a few off-diagonal matrix elements which are related to nonadiabatic transitions between molecular states. In our case we take into account the following transitions:

(i) Localized transitions of the Landau-Zener (LZ) type near the crossing of ${}^1\Pi$ and ${}^3\Sigma^+$ potential curves. These transitions are induced by the spin-orbit interaction and connect states of the same symmetry: ${}^1\Pi(\omega^\sigma=1^\pm) \leftrightarrow {}^3\Sigma^+(\omega^\sigma=1^\pm)$.

(ii) Localized transitions of the Nikitin type in the region of the a-c recoupling. These transitions are induced by the radial motion and connect states of the same symmetry: ${}^3\Sigma^+(\omega^\sigma=1^\pm) \leftrightarrow {}^3\Pi(\omega^\sigma=1^\pm)$ and ${}^3\Sigma^+(\omega^\sigma=0^-) \leftrightarrow {}^3\Pi(\omega^\sigma=0^-)$.

(iii) Nonlocalized transitions of resonance type between the components of the ${}^3\Sigma^+$ potential on the way in, from the crossing point of ${}^3\Sigma^+$ and ${}^1\Pi$ curves to the turning point on the ${}^3\Sigma^+$ curve, and on the way out, from the turning point on the ${}^3\Sigma^+$ curve up to the locking distance R_L. These transitions are induced by the rotational motion and connect degenerate states of different axial symmetry: ${}^3\Sigma^+(\omega^\sigma=0^-) \leftrightarrow {}^3\Sigma^+(\omega^\sigma=1^-)$

Accordingly, the molecular S matrix is constructed from the matrices of adiabatic evolution and the matrices of nonadiabatic transitions. The 12×12 scattering matrix ${}^M\mathbf{S}$ is factored out into 6×6 matrix ${}^M\mathbf{S}^+$ of positive reflection symmetry, and the 6×6 matrix ${}^{M}\mathbf{S}^{-}$ of negative symmetry. The matrix ${}^{M}\mathbf{S}^{+}$ reads

$$
\begin{aligned}
{}^{M}\mathbf{S}^{+}=\lim_{R\to\infty}&[\exp(-ik'R-ikR+iJ\pi+i\pi/2)A(R_N,R)\\
&\times[(\mathbf{N}^{\mathrm{ii}}(R_N)]^{\mathrm{Tr}}\mathbf{A}(R_{\mathrm{LZ}},R_N)\\
&\times[\mathbf{N}^{\mathrm{i}}(R_{\mathrm{LZ}})]^{\mathrm{Tr}}\mathbf{A}^2(R_1,R_{\mathrm{LZ}})\mathbf{N}^{\mathrm{i}}(R_{\mathrm{LZ}})\mathbf{A}(R_{\mathrm{LZ}}R)]. \quad (13)
\end{aligned}
$$

The matrix ${}^{M}\mathbf{S}^{-}$ is slightly more complicated, since it also includes, besides the localized transitions of types (i) and (ii), a nonlocalized transition of type (iii):

$$
\begin{aligned}
{}^{M}\mathbf{S}^{-}=\lim_{R\to\infty}&[\exp(-ik'R-ikR+iJ\pi+i\pi/2)A(R_N,R)\\
&\times[(\mathbf{N}^{\mathrm{ii}}(R_N)]^{\mathrm{Tr}}\mathbf{N}^{\mathrm{iii}}(R_{\mathrm{LZ}},R_N)\mathbf{A}(R_{\mathrm{LZ}},R_N)\\
&\times[\mathbf{N}^{\mathrm{i}}(R_{\mathrm{LZ}})]^{\mathrm{Tr}}[\mathbf{N}^{\mathrm{iii}}(R,R_{\mathrm{LZ}})]^2\mathbf{A}^2(R_t,R_{\mathrm{LZ}})\\
&\times\mathbf{N}^{\mathrm{i}}(R_{\mathrm{LZ}})\mathbf{A}(R_{\mathrm{LZ}},R)]. \qquad (14)
\end{aligned}
$$

Here **A**'s are diagonal matrices of adiabatic evolution between interatomic distances indicated, and **N**'s are the matrices of nonadiabatic transitions labeled by the type of transition. For localized transitions [types (i) and (ii)], the center of the nonadiabaticity region is indicated (R_{LZ} or R_N), while for the nonlocalized transitions [type (iii)] the whole range is indicated. Note that within the accuracy of our calculations, the matrix $\mathbf{N}^{\mathrm{iii}}(R_{\mathrm{LZ}},R_N)$ on the right-hand side of Eq. (14) can be identified with the matrix $\mathbf{N}^{\mathrm{iii}}(R_{\mathrm{LZ}},R_L)$, since both R_N (R_{N0} and R_{N1}) are very close to R_L.

The explicit forms of the matrix elements of A matrices are

$$
\begin{aligned}
A_{c'c}(R_1,R_2)&=\delta_{c'c}\exp[i\Delta_c(R_1,R_2)],\\
\Delta_c(R_1,R_2)&=\frac{1}{\hbar}\int_{R_1}^{R_2}\sqrt{2\mu[E-U_c(R)-(J+1/2)^2/2\mu R^2]}.
\end{aligned}
\qquad (15)
$$

Here c stands for the set of quantum numbers $aj\omega\sigma$ of a molecular state, and the total energy E and the potential energy curves $U_c(R)$ are referred to the common origin. Note also that the centrifugal energy in the molecular region is determined by the total angular momentum J rather than by the relative angular momenta l,l', even in the asymptotic region $R\to\infty$. The switching from J to l,l' which is necessary to insure correct boundary conditions for the scattering wave function, is accomplished by the locking matrices. The matrices of nonadiabatic transitions $\mathbf{N}^{\mathrm{i}}$, $\mathbf{N}^{\mathrm{ii}}$, and $\mathbf{N}^{\mathrm{iii}}$ are of a block-diagonal form, with blocks consisting of 2×2 matrices.

For the type-(i) transition, ${}^{1}\Pi(\omega^{\sigma}=1^{\pm})\leftrightarrow{}^{3}\Sigma^{+}(\omega^{\sigma}=1^{\pm})$, the coupling between adiabatic states, that emerge from the diabatic states ${}^{1}\Pi$ and ${}^{3}\Sigma^{+}$ under the action of the spin-orbit interaction, is described by the Landau-Zener model. It was found earlier [14] that the motion here is almost diabatic, and the transition probability between diabatic states p' is

$$
p'=\frac{2\pi V_{\mathrm{so}}^2}{\Delta F_{\mathrm{LZ}}\sqrt{(2/\mu)[E-U_{\mathrm{LZ}}-(J+1/2)^2/2\mu R_{\mathrm{LZ}}^2]}} \qquad (16)
$$

Here V_{so} is the matrix element of the spin-orbit interaction between ${}^{1}\Pi(\omega^{\sigma}=1^{\pm})$ and ${}^{3}\Sigma^{+}(\omega^{\sigma}=1^{\pm})$ states, R_{LZ} is the crossing distance between these potential curves, U_{LZ} is the potential energy at the crossing distance, and ΔF_{LZ} is the difference in slopes of these potentials at the crossing point. The $(N^{i}_{c'c})$ matrix actually assumes the form

$$
(N^{\mathrm{i}}_{c'c})=\begin{pmatrix}\sqrt{p'}\exp(-i\pi/4) & 1\\ -1 & \sqrt{p'}\exp(i\pi/4)\end{pmatrix}, \qquad (17)
$$

where $p'\ll 1$.

In region (ii), the 2×2 blocks of the N matrices have a standard form for the Nikitin exponential model [15,38]:

$$
(N^{\mathrm{ii}}_{c'c})=\begin{pmatrix}\sqrt{1-P}\exp(-i\varphi) & \sqrt{P}\exp(i\psi)\\ -\sqrt{P}\exp(-i\psi) & \sqrt{1-P}\exp(i\varphi)\end{pmatrix}, \qquad (18)
$$

where P is the transition probability between adiabatic molecular states, and φ and ψ are certain phases that depend on the type of the transition. In Eq. (18), the transition probability depends on two parameters, related to the spacing of potential curves far from the coupling region, ΔE, the logarithmic derivative of the difference of two adiabatic potentials at the center of the coupling region, $\alpha/2$, the mixing angle $\vartheta/2$, and the relative velocity of atoms at the center of the coupling region, ν_p. The parameters in question are [15,38]

$$
\varsigma=\Delta E/(\hbar\alpha\nu_p), \quad \varsigma_p=\varsigma\,\sin^2(\vartheta/2). \qquad (19)
$$

In terms of these parameters, the expressions for the transition probability and phases read

$$
P=\exp(-\pi\varsigma_p)\,\frac{\sinh(\pi\varsigma-\pi\varsigma_p)}{\sinh(\pi\varsigma)} \qquad (20)
$$

and

$$
\begin{aligned}
\varphi&=\gamma(\varsigma_p)-\gamma(\varsigma),\\
\psi&=\gamma(\varsigma-\varsigma_p)-\gamma(\varsigma)-\left\{2\sqrt{\varsigma\varsigma_p}-(\varsigma-\varsigma_p)\ln\frac{\sqrt{\varsigma}+\sqrt{\varsigma_p}}{\sqrt{\varsigma}-\sqrt{\varsigma_p}}\right\},
\end{aligned}
\qquad (21)
$$

where

$$
\gamma(z)=\pi/4-\arg\,\Gamma(1+iz)+z(\ln z-1). \qquad (22)
$$

For the type-(ii) transition, the interaction between adiabatic states belonging to the intermediate a-c Hund case arises from the coupling by the radial motion of the partners within a small range of interatomic distances close to $R=R_N$. Actually, there are two different cases here: one corresponding to $\cos\vartheta=0$ [transitions ${}^{3}\Sigma^{+}(\omega^{\sigma}=1^{\pm})\leftrightarrow{}^{3}\Pi(\omega^{\sigma}=1^{\pm})$], and the other to $\cos\vartheta=-\frac{1}{3}$ [transition ${}^{3}\Sigma^{+}(\omega^{\sigma}=0^{-})\leftrightarrow{}^{3}\Pi(\omega^{\sigma}=0^{-})$], with slightly different values of R_N. In both cases, the general equations (18)–(22) apply, in which ΔE is identified with $\Delta\varepsilon_{21}$ for the first case and with $\Delta\varepsilon_{20}$ for the second case. We note, in passing, that the transition probability for the case $\cos\vartheta=0$ coincides with the Rosen-Zener-Demkov formula, while, in the limit $\vartheta\ll 1$, the Landau-Zener formula is recovered.

Finally, for the type-(iii) transition, the interaction between adiabatic states 0^- and 1^- of the Hund *a* nomenclature for the ${}^3\Sigma^+$ multiplet is due to the rotational coupling between degenerate states. The matrix $\mathbf{N}^{\mathrm{iii}}$ is simply the 2×2 matrix of rotation through angle Φ, which is covered by the molecular axis during the excursion of the system along R_1/R_2 interval (with R_1 and R_2 being appropriate distances, as implied by Eq. (14)). The explicit expression for N^{iii}, when it is supposed to act on the column vector $(|1^-\rangle,|0^-\rangle)$, reads

$$(N^{\mathrm{iii}}_{c'c})=\begin{pmatrix} \cos\Phi & -i\sin\Phi \\ -i\sin\Phi & \cos\Phi \end{pmatrix}. \tag{23}$$

The rotational mixture of states can, in principle, have a significant effect on the overall nonadiabatic transition probability [39].

The molecular scattering matrix ${}^M\mathbf{S}$ can now be synthesized from **A** and **N** matrices. Sandwiched between C matrices, ${}^M\mathbf{S}$ yields the scattering matrix S in the J-helicity representation.

VI. DIFFERENTIAL AND INTEGRAL CROSS SECTIONS

Calculation of differential cross sections in the quasiclassical approximation is facilitated by two simplifications which are related to the structure of the J-helicity S matrix and the stationary-phase solutions of the integrals that define the scattering amplitude. As discussed at length in Ref. [15], each element of the S matrix can be represented as a sum over different classical paths γ that connect the initial and final states and run on different portions of adiabatic potential curves with the relative angular momentum J (or impact parameter b related to J as $kb=J+\frac{1}{2}$):

$$S_{c'c}(J)=\sum_{\gamma} s^{\gamma}_{c'c}(J)\exp[2i\delta^{\gamma}_{c'c}(J)]. \tag{24}$$

The reason behind the splitting $S_{c'c}(J)$ into several components is that each of them features quite specific behavior: a much stronger dependence of the exponential on J compared to that of the preexponential factor. The exponents, which are similar to the WKB phase shifts for elastic scattering, can be recovered from the classical deflection functions $\eta^{\gamma}_{c'c}(J)$, while the preexponential factors $s^{\gamma}_{c'c}(J)$ contains parameters that enter into the N and C matrices.

For our case, the number of different paths can be reduced to two, if the collision energy is noticeably higher than the spin-orbit interaction. Then the paths that correspond to different fine-structure exit channels coalesce, and the sum in Eq. (24) will be over two paths. Let the deflection functions for these paths be $\eta^{1}_{\Sigma\Pi}(b)$ and $\eta^{2}_{\Sigma\Pi}(b)$. The first path corresponds to the entrance along the ${}^1\Pi$ potential curve to the separation R_{LZ}, then the further approach on the ${}^3\Sigma^+$ potential curve until the turning point $R_t({}^3\Sigma^+)$ and the recede along this curve until it merges with the manifold of ${}^3\Pi$ state. For this path, the system moves at $R<R_{\mathrm{LZ}}$ across the ${}^3\Sigma^+$ potential. Therefore, we adopt notation $\eta^{1}_{\Sigma\Pi}=\eta^{\Sigma}_{\Sigma\Pi}$. The second path runs on the ${}^1\Pi$ potential curve until the turning point $R_t({}^1\Pi)$, then recedes, and after reaching the crossing point R_{LZ} continues on the ${}^3\Sigma^+$ potential; the respective deflection function is $\eta^{2}_{\Sigma\Pi}=\eta^{\Pi}_{\Sigma\Pi}$. The curves representing two functions $\eta^{\Sigma}_{\Sigma\Pi}(b)$ and $\eta^{\Pi}_{\Sigma\Pi}(b)$ meet at a certain point b_{LZ}, and form two branches of a single deflection function $\eta_{\Pi\Sigma}(b)$ for the inelastic scattering [15]. We note in passing that if the collision energy is noticeably higher than the attraction energy for the ${}^1\Pi$ potential curve at R_{LZ}, then b_{LZ} is close to R_{LZ}. The deflection function $\eta_{\Pi\Sigma}(b)$ for the potentials shown in Fig. 1 and for a collision energy of 1 eV is represented in Fig. 2.

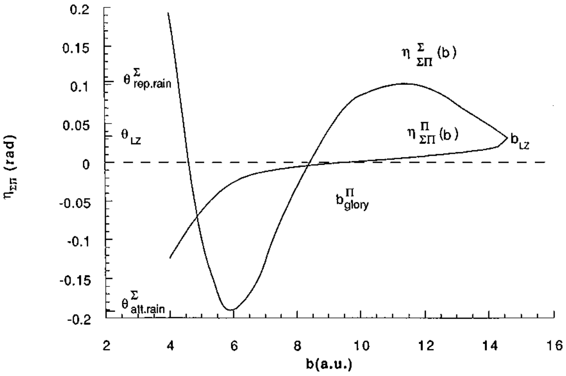

FIG. 2. Deflection function for the inelastic collisions $\mathrm{Ca}({}^1P_1)+\mathrm{He}\rightarrow\mathrm{Ca}({}^3P_j)+\mathrm{He}$ at a collision energy 1 eV.

We now turn to a calculation of the scattering amplitudes and cross sections. Consider first scattering through classical angles. The representation of the S matrix in the form given by Eq. (24) is suitable for calculation of the scattering amplitudes in the stationary-phase approximation. In this approximation, one looks at a given θ for a value of J (or b) at which the total phase composed of $\mp\theta J$ and $2\delta^{\gamma}_{c'c}(J)$ has an extremum. These values of J are found from the equation:

$$|\eta^{\gamma}_{c'c}(J)|=\theta, \tag{25}$$

and each roots of this equation, $J=J_{\Gamma}(\theta)$, defines a trajectory Γ which is scattered through angle θ. Because of the complicated shape of the deflection function and the contribution of positive and negative values of η to the same value of θ (recall that the range of θ is $0/\pi$) the number of solutions to Eq. (25) that determine different trajectories Γ is usually larger than the number of paths γ that enter into sum (24). In this approximation, the scattering amplitude $F_{c'c}(\theta)$ is represented as a sum over different trajectories Γ:

$$F_{c'c}(\theta)=\sum_{\Gamma}\sqrt{q^{\Gamma}_{c'c}(\theta)}\,\exp[2i\Phi^{\Gamma}_{c'c}(\theta)+i\Psi^{\Gamma}_{c'c}]. \tag{26}$$

All the quantities that enter into the right-hand side of Eq. (26) can be recovered from the classical deflection functions $\eta^{\Gamma}_{c'c}(b)$ of the inelastic event, transition probabilities, and phases that enter into the matrices of nonadiabatic transitions and parameters of the locking matrix. For instance, for the deflection function shown in Fig. 2, the number of trajectories is six for $\theta<\theta^{\Sigma}_{\mathrm{rep.rain}}$, four for $\theta^{\Sigma}_{\mathrm{rep.rain}}<\theta<\theta^{\Sigma}_{\mathrm{att.rain}}$, and two for $\theta^{\Sigma}_{\mathrm{att.rain}}<\theta$ [the indices rep.rain and att.rain with index Σ stand for the repulsive and attractive rainbows at the Σ branch of the function $\eta_{\Sigma\Pi}(b)$].

TABLE I. Parameters used for the calculation of the differential cross sections for the inelastic scattering $\mathrm{Ca}({}^1P_{1,n})+\mathrm{He}\rightarrow\mathrm{Ca}({}^3P_{j,n'})+\mathrm{He}$ (in a.u.) at a collision energy of 1 eV.

Collision energy E	3.675×10^{-2}
Initial wave vector k	22.06
Reduced mass μ	6686
Relative velocity v	0.003 32
Landau-Zener crossing distance R_{LZ}	14.6
Pseudocrossing distance for $\Omega=1$ states, R_{N1}	22
Pseudocrossing distance for $\Omega=0^-$ states, R_{N0}	21.2
Locking angle, α_L	$0.058b$
Slipping probability, s	$0.012b$
Energy spacing ${}^1P_1-{}^3P_2$	0.714×10^{-3}
Energy spacing ${}^3P_2-{}^3P_1$	0.93×10^{-4}
Energy spacing ${}^3P_1-{}^3P_0$	0.32×10^{-4}
Landau-Zener parameter $\sqrt{p'}$ for head-on collision	0.11

When expression (26) is used for the calculation of the differential cross section through classical angles [Eqs. (3)–(5)], the latter will assume the form

$$q_{c'c}(\theta)=\sum_{\Gamma} q^{\Gamma}_{c'c}(\theta)+2\sum_{\Gamma\neq\Gamma'}\sqrt{q^{\Gamma}_{c'c}(\theta)q^{\Gamma'}_{c'c}(\theta)}\times\cos[2\Delta\Phi^{\Gamma,\Gamma'}_{c'c}(\theta)+\Delta\Psi^{\Gamma,\Gamma'}_{c'c}]. \tag{27}$$

The first sum on the right-hand side of Eq. (27) represents a contribution from fluxes traveling along different trajectories; usually this term varies slowly and regularly with θ. It can be written schematically as

$$q^{\Gamma}_{c'c}(\theta)=L_{c'c}[b^{\Gamma}_{c'c}(\theta)]T_{c'c}[b^{\Gamma}_{c'c}(\theta)]q^{\Gamma,\mathrm{el}}_{c'c}(\theta), \tag{28}$$

where the factor $L_{c'c}$ comes from a bilinear combination of locking matrices, $T_{c'c}$ comes from matrices of nonadiabatic transitions, and $q^{\Gamma,\mathrm{el}}_{c'c}(\theta)$ are similar to the classical elastic cross sections

$$q^{\Gamma,\mathrm{el}}_{c'c}(\theta)=\frac{1}{\sin\theta}\,b^{\Gamma}_{c'c}(\theta)\left|\frac{db^{\Gamma}_{c'c}(\theta)}{d\theta}\right|. \tag{29}$$

The form of the arguments in functions $L_{c'c}$ and $T_{c'c}$ is intended to emphasize the fact that their θ dependence should be recovered from a particular trajectory Γ with the impact parameter $b^{\Gamma}_{c'c}(\theta)$.

The second sum on the right-hand side of Eq. (27) represents the interference contribution from waves traveling along different trajectories. The phase differences $\Delta\Phi^{\Gamma,\Gamma'}_{c'c}(\theta)$ are completely defined by the deflection function, and are supposed to be large (applicability of the stationary-phase approximation). The phase differences $\Delta\Psi^{\Gamma,\Gamma'}_{c'c}$ arise from combination of the phases entering into **C** and **N** matrices, and also from the stationary phase integration.

When some $\Delta\Phi^{\Gamma,\Gamma'}_{c'c}(\theta)$ are not large, the stationary-phase approximation breaks down, and some terms in the first and second sums show divergence. Then they can be combined and replaced by a certain uniform approximation which is not divergent. The important property of this approximation is that it does not require any additional information on the scattering. In our calculations we used the Airy uniform approximation [15] to calculate the cross sections close to the rainbow angles $\theta^{\Sigma}_{\mathrm{rep.rain}}$ and $\theta^{\Sigma}_{\mathrm{att.rain}}$. Actually, at an energy of 1 eV, the deflection function can be calculated in the high-energy approximation [15] up to scattering angles of about 0.15 rad, where the cross sections are not too small.

Consider now the scattering through angles in the diffraction region. In this region the scattering amplitude is given by Eq. (6). A simplified version of this expression can be obtained if one solves the integral over J in the stationary-phase approximation. In this case, the possible classical trajectories correspond to nondeviated trajectories; that is, the respective J_{Γ} values are found from the equation

$$|\eta^{\gamma}_{c'c}(J)|=0. \tag{30}$$

The angle dependence of the scattering amplitude is given by a linear combination of the Bessel functions:

$$F_{c'c}(\theta)=-i\sqrt{2\pi k}\sum_{\Gamma} b_{\Gamma}|d\eta^{\Gamma}_{c'c}(b)/db|^{-1/2}_{b=b_{\Gamma}}\times\exp(i\pi\sigma^{\Gamma}_{c'c}/4)G^{\Gamma}_{c'c}(\theta,J_{\Gamma}), \tag{31}$$

where

$$G^{\Gamma}_{c'c}(\theta,J_{\Gamma})\equiv G^{\Gamma}_{a'j'n';ajn}(\theta,J_{\Gamma})=\sum_{m'mv'v}\Delta^{j'}_{m'n'}\Delta^{j'}_{m'v'}\times\Delta^{j}_{mn}\Delta^{j}_{mv}i^{m-m'}J_{m'-m}(\theta J_{\Gamma})\times\exp(-i\pi v')S_{a'j'v';ajv}(J_{\Gamma}), \tag{32}$$

and $\sigma^{\Gamma}_{c'c}=\mathrm{sgn}(d\eta^{\Gamma}_{c'c}(b)/db)$ at $b=b_{\Gamma}$.

The values of parameters which were used for the calculation of the cross section are given in Table I. The calculated cross sections are presented in Figs. 3–10. In these figures, positive values of θ correspond to scattering to the

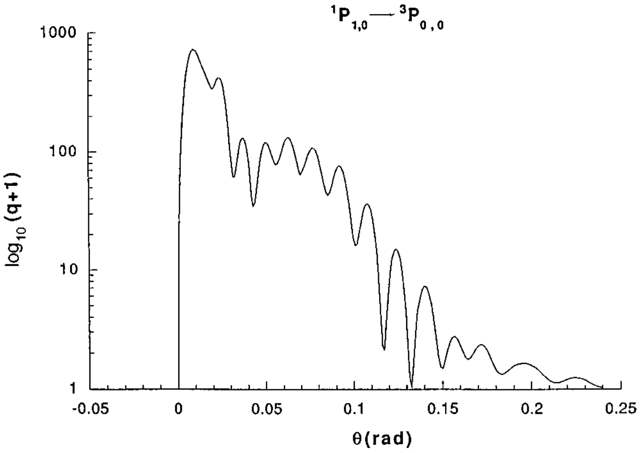

FIG. 3. Differential cross section q for Ca+He scattering (in a.u.) for the $^1P_{1,0} \rightarrow {}^3P_{0,0}$ transition. Positive scattering angles θ correspond to scattering to the right, and negative angles to scattering to the left. Since for this transition the right-left scattering asymmetry is absent, only the scattering to the right is shown.

right, and negative values correspond to scattering to the left. In all these figures, we single out the following four regions of scattering angles.

(i) $\theta \leqslant \theta_{\mathrm{LZ}} = 0.03$. Here the main contribution to the cross section comes from the scattering on $^1\Pi$ potential.

(ii) $\theta_{\mathrm{LZ}} \leqslant \theta \leqslant \theta^{\Sigma}_{\mathrm{rep.rain}} = 0.10$. In this region, the main contribution to the cross section comes from the scattering on the potential barrier of the $^3\Sigma^+$ potential.

(iii) $\theta^{\Sigma}_{\mathrm{rep.rain}} \leqslant \theta \leqslant \theta^{\Sigma}_{\mathrm{att.rain}} = 0.19$. Here, the main contribution to the cross section comes from the scattering on the potential well of the $^3\Sigma^+$ potential.

(iv) $\theta^{\Sigma}_{\mathrm{att.rain}} \leqslant \theta$. The cross section is determined by the interference of two waves, one scattered by the repulsive branch of the $^3\Sigma^+$ potential and the other scattered by the attractive branch of the $^1\Pi$ potential.

Considering the above, one easily understands why all the cross sections drop at $\theta \approx \theta^{\Sigma}_{\mathrm{rep.rain}} = 0.10$ (rainbow scattering on the barrier of the $^3\Sigma^+$ potential). Another general feature is the increase of the cross sections near the Landau-Zener angle $\theta_{\mathrm{LZ}} = 0.03$. This is related to the constructive interference of waves scattered on $^3\Sigma^+$ and $^1\Pi$ potentials, and the increase in the Landau-Zener transition probability at impact parameters close to b_{LZ}. At still smaller angles, the increase of the cross sections is related to a graduate transition to the glory scattering.

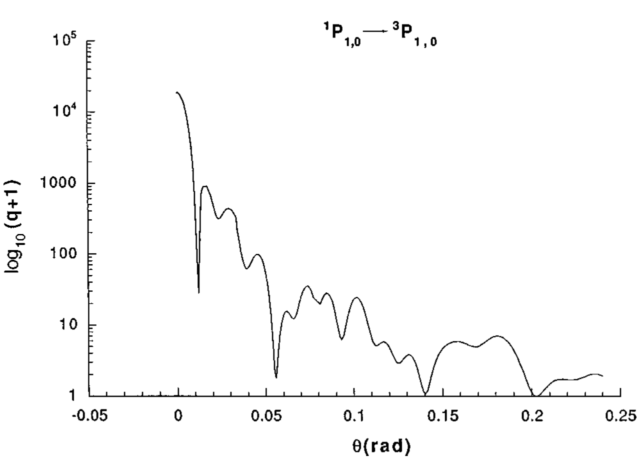

FIG. 4. Differential cross section q for Ca+He scattering (in a.u.) for the $^1P_{1,0} \rightarrow {}^3P_{1,0}$ transition. Positive scattering angles θ correspond to the scattering to the right, and negative angles to scattering to the left. Since for this transition the right-left scattering asymmetry is absent, only the scattering to the right is shown.

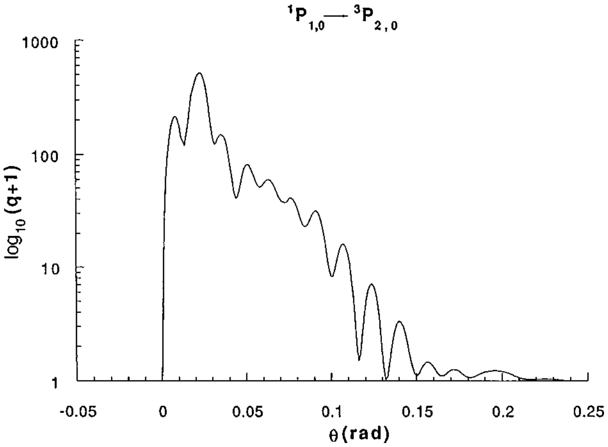

FIG. 5. Differential cross section q for Ca+He scattering (in a.u.) for the $^1P_{1,0} \rightarrow {}^3P_{2,0}$ transition. Positive scattering angles θ correspond to scattering to the right, and negative angles to scattering to the left. Since for this transition the right-left scattering asymmetry is absent, only the scattering to the right is shown.

The difference in various cross sections is mainly due to the Coriolis interaction, which acts in the region of locking at large interatomic distances, and also in the region of mixing components of the $^3\Sigma^+$ state at $R < R_L$. The largest cross sections correspond to the initial zero J-helicity state, since this state is already locked to the molecular axis, and becomes completely the $^1\Pi_{1^-}$ molecular state.

Compare now cross sections for transitions $^1P_{1,0} \rightarrow {}^3P_{0,0}$, $^1P_{1,0} \rightarrow {}^3P_{1,0}$, $^1P_{1,0} \rightarrow {}^3P_{2,0}$, and $^1P_{1,0} \rightarrow {}^3P_{2,2}$. Consider first the region of classical angles, (Figs. 3–10). Here the cross section for transition $^1P_{1,0} \rightarrow {}^3P_{1,0}$ is considerably smaller compared to other cross sections. This is ex-

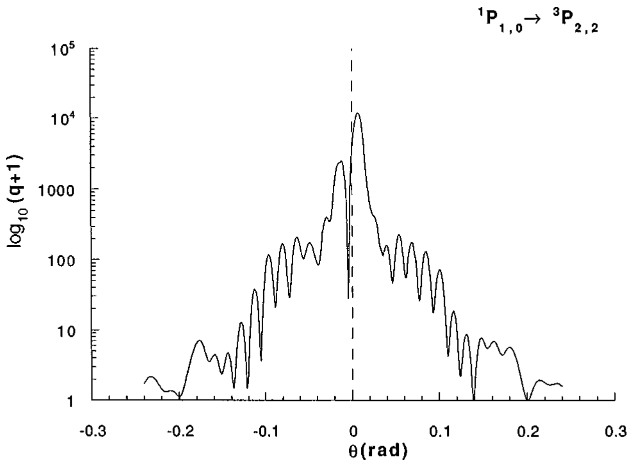

FIG. 6. Differential cross section q for Ca+He scattering (in a.u.) for the $^1P_{1,0} \rightarrow {}^3P_{2,2}$ transition. Positive scattering angles θ correspond to scattering to the right, and negative angles to scattering to the left.

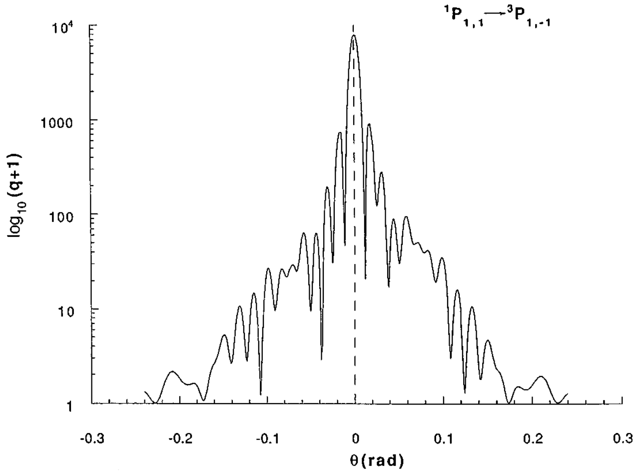

FIG. 7. Differential cross section q for Ca+He scattering (in a.u.) for the $^1P_{1,1} \rightarrow {}^3P_{1,-1}$ transition. Positive scattering angles θ correspond to scattering to the right, and negative angles to scattering to the left.

plained in the following way. The scattering in this range of angles is driven by the motion on the $^3\Sigma^+$ potential, where there exists a considerable Coriolis mixing between the $^3\Sigma^+_{1^-}$ component (populated in the Landau-Zener transition on the way in) and the $^3\Sigma^+_{0^-}$, component at $R < R_{\mathrm{LZ}}$. This mixing leads to a considerable depletion of the state $^3\Sigma^+_{1^-}$, so that the nonadiabatic transition $^3\Sigma^+_{1^-} \rightarrow {}^3\Pi_{1^-}$ which occurs after the system crosses R_{LZ} on the way out, finally brings the system to the $^3P_{10}$ state.

Turn now to smaller scattering angles. Here the cross section for the transition $^1P_{1,0} \rightarrow {}^3P_{1,0}$ is the largest one exhibiting a peak at zero angles. The cross section for transition $^1P_{1,0} \rightarrow {}^3P_{2,2}$ is smaller, and shows a large asymmetry. The cross sections for two other transitions, $^1P_{1,0} \rightarrow {}^3P_{0,0}$ and $^1P_{1,0} \rightarrow {}^3P_{2,0}$, are still smaller and vanish at $\theta = 0$. These features are explained by the fact that in this range of angles, the scattering is driven mainly by the motion on the $^1\Pi$ potential (hence the initial high population of the $^1\Pi_{1^-}$ is not considerably depleted), and the peak is due to the contribution of the diffraction term $J_0(kb^{\Pi}_{\mathrm{glory}}\theta)$ with $b^{\Pi}_{\mathrm{glory}} = 9.8$ (see Fig. 2), since other contributions, proportional to $J_{m'-m}(kb^{\Pi}_{\mathrm{glory}}\theta)$ with $m' - m \neq 0$, vanish at $\theta = 0$. On the other hand, the diffraction term $J_0(kb^{\Pi}_{\mathrm{glory}}\theta)$ does not contribute to the cross sections for the transitions $^1P_{1,0} \rightarrow {}^3P_{0,0}$ and $^1P_{1,0} \rightarrow {}^3P_{2,0}$ since $\Delta^1_{00} = \Delta^2_{\pm 10} = 0$. As for the transition $^1P_{1,0} \rightarrow {}^3P_{2,2}$, the large asymmetry of the cross section is due to the strong manifestation of the locking.

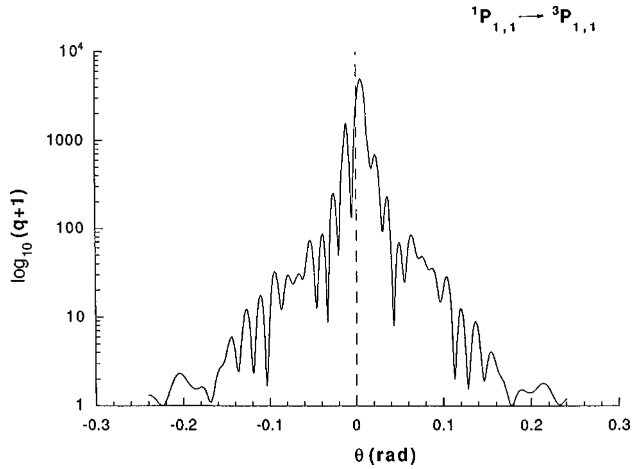

FIG. 8. Differential cross section q for Ca+He scattering (in a.u.) for the $^1P_{1,1} \rightarrow {}^3P_{1,1}$ transition. Positive scattering angles θ correspond to scattering to the right, and negative angles to scattering to the left.

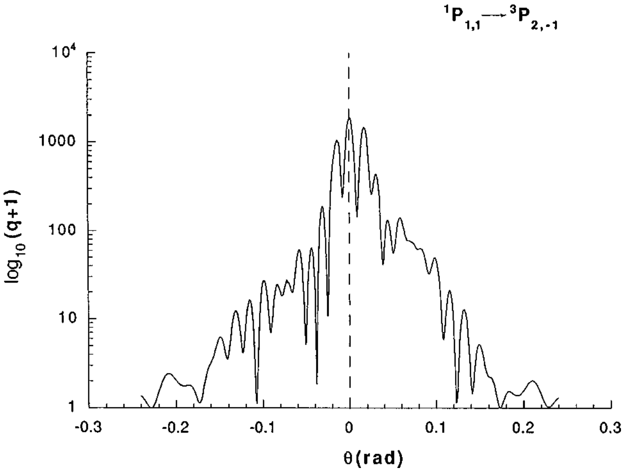

FIG. 9. Differential cross section q for Ca+He scattering (in a.u.) for the $^1P_{1,1} \rightarrow {}^3P_{2,-1}$ transition. Positive scattering angles θ correspond to scattering to the right, and negative angles to scattering to the left.

In general, the azimuthal scattering asymmetry shows itself in two features: in a shift of the scattering pattern along θ axis, and in a difference in heights of the secondary maxima situated at both sides from the main maximum. The shift $\Delta\theta_{c'c}$ in the cross section for transition $c \rightarrow c'$ is roughly determined by an equation

$$\Delta\theta_{c'c} = \frac{d\alpha_{L,c'}}{dJ}\, n' + \frac{d\alpha_{L,c}}{dJ}\, n. \tag{33}$$

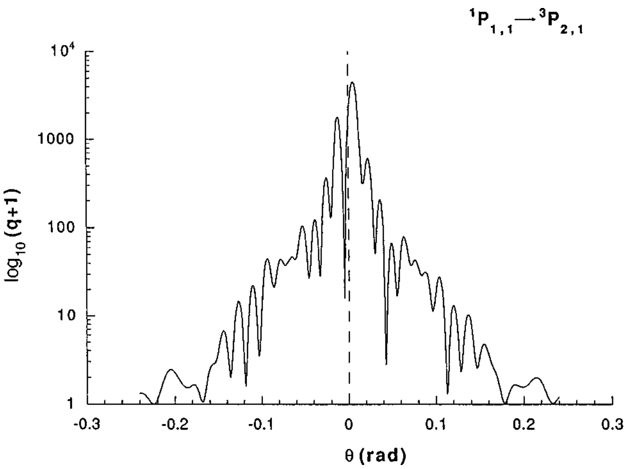

FIG. 10. Differential cross section q for Ca+He scattering (in a.u.) for the $^1P_{1,1} \rightarrow {}^3P_{2,1}$ transition. Positive scattering angles θ correspond to scattering to the right, and negative angles to scattering to the left.

TABLE II. Nonvanishing Zeeman-specific cross sections for the inelastic scattering $\mathrm{Ca}(^1P_{1,n})+\mathrm{He}\rightarrow\mathrm{Ca}(^3P_{j,n'})+\mathrm{He}$.

Collision event	$\sigma^{\text{right+left}}$	$\Delta\sigma^{\text{right}-\text{left}}$	A
$^1P_{1,0}\rightarrow{}^3P_{0,0}$	1.26	0	0
$^1P_{1,0}\rightarrow{}^3P_{1,0}$	1.80	0	0
$^1P_{1,0}\rightarrow{}^3P_{2,0}$	0.92	0	0
$^1P_{1,0}\rightarrow{}^3P_{2,2}$	2.94	0.54	0.18
$^1P_{1,1}\rightarrow{}^3P_{1,-1}$	1.11	0.21	0.19
$^1P_{1,1}\rightarrow{}^3P_{1,1}$	1.17	0.36	0.31
$^1P_{1,1}\rightarrow{}^3P_{2,-1}$	1.23	0.44	0.35
$^1P_{1,1}\rightarrow{}^3P_{2,1}$	1.24	0.11	0.09

Since two derivatives are close to each other, a noticeable shift exists for transitions with $n'+n=2$, that is, for transitions $^1P_{1,0}\rightarrow{}^3P_{2,2}$, $^1P_{1,1}\rightarrow{}^3P_{2,1}$, and $^1P_{1,1}\rightarrow{}^3P_{1,1}$.

The overall intensity of the scattering to the right in the scattering plane can be characterized by integral ‘‘in-half-plane’’ cross sections $\sigma_{a'j'n';ajn}$, which represent differential cross section integrated only over the polar angle θ:

$$\sigma_{a'j'n';ajn}=\int_0^{\pi}q_{a'j'n';ajn}(\theta)\sin\,\theta d\theta. \tag{34}$$

The overall intensity of the scattering to the left is given by a similar expression in which n',n is replaced by $-n'$, $-n$, and the total intensity for scattering both to the right and left is given by the sum of two in-half-plane cross sections:

$$\sigma^{\text{right+left}}_{a'j'n';ajn}=\sigma_{a'j'n';ajn}+\sigma_{a'j'-n';aj-n}; \tag{35}$$

see Table II. The right-left scattering asymmetry can be then characterized by the difference of two in-half-plane cross sections

$$\Delta\sigma^{\text{right}-\text{left}}_{a'j'n';ajn}=\sigma_{a'j'n';ajn}-\sigma_{a'j'-n';aj-n}, \tag{36}$$

or by the ratio

$$A_{a'j'n';ajn}=\frac{\Delta\sigma^{\text{right}-\text{left}}_{a'j'n';ajn}}{\sigma^{\text{right+left}}_{a'j'n';ajn}}, \tag{37}$$

see Table II. If the in-half-plane cross section $\sigma_{a'j'n';ajn}$ is summed over final j',n' states, it will give a total in-half-plane cross section for the scattering to the right in the collision plane out of the initial state ajn:

$$\sigma_{a';ajn}=\sum_{j'n'}\sigma_{a'j'n';ajn}; \tag{38}$$

see Table III. Similarly, $\sigma_{a';aj-n}$ is the scattering to the left from the same initial state ajn. Finally, if $\sigma_{a';ajn}$ is averaged over all initial projections n, it yields an azimuthal-independent quantity. When multiplied by 2π (a result of integration over the azimuthal angle), it yields the total integral cross section for inelastic scattering $^1P_1\rightarrow{}^3P_j$, all j:

$$\sigma(^1P_1\rightarrow{}^3P_j,\ \text{all}\ j)=\frac{2\pi}{3}\sum_{j'n'n}\sigma_{a'j'n';ajn}$$

TABLE III. The total in-half-plane cross sections for the scattering to the right in collisions of helicopter-polarized atoms $\mathrm{Ca}(^1P_{1,n}\rightarrow{}^3P,\ \text{all}\ j',n')$ and the total integral cross section in collisions of unpolarized atoms $\mathrm{Ca}(^1P_{1,\text{unpol}}\rightarrow{}^3P,\ \text{all}\ j',n')$ (last row).

Collision event	Cross section
$^1P_{1,1}\rightarrow{}^3P$, all j',n'	2.99
$^1P_{1,0}\rightarrow{}^3P$, all j',n'	4.93
$^1P_{1,-1}\rightarrow{}^3P$, all j',n'	1.81
$^1P_{1,\text{unpol}}\rightarrow{}^3P$, all j',n'	20.3

$$=\frac{\pi}{3}\sum_{j'n'n}\sigma^{\text{right+left}}_{a'j'n';ajn}$$

$$=\frac{2\pi}{3}\sum_{n}\sigma_{a';ajn}; \tag{39}$$

see Table II. Of course, $\sigma(^1P_1\rightarrow{}^3P_j,\ \text{all}\ j)$ is directly expressed via the scattering matrix

$$\sigma(^1P_1\rightarrow{}^3P_j,\ \text{all}\ j)=\frac{2\pi}{3}\int_0^{\infty}\sum_{j'v'v}|S_{a'j'v';ajv}(J)|^2\frac{JdJ}{k^2}. \tag{40}$$

VII. CONCLUSION

In this paper, we presented a quasiclassical theory of inelastic, spin-changing collisions of an excited $\mathrm{Ca}(4s5p,{}^1P_1)$ atom with He, at a collision energy of 1 eV. All Zeeman-specific differential cross sections for transitions for helicopter-oriented atoms are peaked at small angles. This feature is completely different from the small-angle elastic scattering which comes from collisions with large impact parameters. In our case, the maximum value of the impact parameter is determined by the access to the Landau-Zener crossing between the $^1\Pi_1$ and $^3\Sigma^+$ potential curves which steer the nuclear motion in the region of a quasimolecule. The small scattering angles arise as a result of interplay between attractive and repulsive interatomic motion in the range of impact parameters where the quasiclassical approximation to the scattering matrix is well founded. The range of scattering angles splits into the range of classical angles and the range of diffraction angles. For the latter range, the effects of quantum scattering are shown by an out-of-plane contribution of the incident wave into the in-plane scattering amplitudes. However, all the information which is needed for a calculation of cross sections is recovered from classical deflection functions, and matrices of the localized nonadiabatic transitions: the Landau-Zener coupling for the crossing $^1\Pi_1$ and $^3\Sigma^+_1$ potential curves, the Demkov and Nikitin coupling for $^3\Sigma^+_\Omega$ and $^3\Pi_\Omega$ potential curves, the nonlocalized Coriolis coupling for the components of the $^3\Sigma^+$ potential curve, and the locking coupling for the molecular potential curves merging to the same initial and final atomic states.

We have shown that the locking phenomenon is responsible for a noticeable right-left asymmetry of the differential cross sections for the scattering of helicopter-oriented atoms. We also identified the parameters which are responsible for the scattering asymmetry and the absolute values of the cross sections, including those entering into the locking matrix (locking angles and slipping probabilities).

The quasiclassical approximation used makes the connection between the input—adiabatic molecular states—and output—differential cross sections—particularly easy, since they are interrelated by the classical deflection functions for inelastic scattering and standard models of nonadiabatic coupling. This leaves the possibility to update the results when better potential curves are available, or to modify them if one replaces He by Ne. The results of calculations yield information which is necessary for planning experiments on the measurements of the Zeeman-specific differential inelastic scattering of an excited Ca atom.

ACKNOWLEDGMENTS

This work was supported in part by the Russian Foundation of Basic Research (Grant No. 96-03-33679-a). A.D. gratefully acknowledges the support of the Japan Society for Promotion of Science during his stay at the Tohoku University, where this work was completed, the hospitality of Professor Y. Sato, and valuable discussions on adiabatic potentials with Dr. A. Zagrebin. E.D. and E.N. thank the Technion VPR Fund, Promotion of Sponsored Research, and the Center for Interdisciplinary Research of Bielefeld University in the Research Group ‘‘Interaction of Oriented Molecules’’ for the support of this work, and for their hospitality.

---

[1] E. I. Dashevskaya, F. Masnou-Seeuws, and E. E. Nikitin, J. Phys. B **29**, 395 (1996).

[2] E. I. Dashevskaya, F. Masnou-Seeuws, and E. E. Nikitin, J. Phys. B **29**, 415 (1996).

[3] E. I. Dashevskaya, E. E. Nikitin, F. Perales, and J. Baudon, J. Phys. B **30**, 703 (1997).

[4] M. Philippe, F. Masnou-Seeuws, and P. Valiron, J. Phys. B **12**, 2493 (1979).

[5] G. Carter, D. Pritchard, M. Kaplan, and Y. Ducas, Phys. Rev. Lett. **35**, 1144 (1975).

[6] F. Perales, Ph.D. thesis, Université de Paris XI, 1990 (unpublished).

[7] M. O. Hale and S. R. Leone, J. Chem. Phys. **79**, 3352 (1983).

[8] H.-Y. Yuh and P. J. Dagdigian, Phys. Rev. A **28**, 63 (1983).

[9] M. O. Hale, I. V. Hertel, and S. R. Leone, Phys. Rev. Lett. **53**, 2296 (1984).

[10] W. Bussert, B. Neuschaefer, and S. R. Leone, J. Chem. Phys. **87**, 3833 (1987).

[11] K. C. Lin, P. D. Kleiber, J. X. Wang, W. C. Stwalley, and S. R. Leone, J. Chem. Phys. **89**, 4771 (1988).

[12] S. Ananthamurthy, P. D. Kleiber, W. C. Stwalley, and K. C. Lin, J. Chem. Phys. **90**, 7605 (1989).

[13] A. Z. Devdariani and A. L. Zagrebin, Khim. Fiz. **1**, 947 (1982); **1**, 1141 (1982) [Sov. J. Chem. Phys. **1**, 1638 (1984); **1**, 1980 (1984)].

[14] A. Z. Devdariani and A. L. Zagrebin, Chem. Phys. Lett. **131**, 197 (1986).

[15] E. E. Nikitin and S. Ya. Umanskii, *Theory of Slow Atomic Collisions* (Springer, Berlin, 1984).

[16] G. K. Ivanov, Opt. Spektrosk. **40**, 965 (1976) [Opt. Spektrosc. **40**, 554 (1976)].

[17] A. Z. Devdariani, A. L. Zagrebin, and K. B. Blagoev, Ann. Phys. (Paris) **14**, 467 (1989).

[18] A. Z. Devdariani and A. L. Zagrebin, Khim. Fiz. **5**, 147 (1986) [Sov. J. Chem. Phys. **5**, 237 (1989)].

[19] A. Z. Devdariani, A. L. Zagrebin, and M. G. Lednev, Opt. Spektrosk. **65**, 573 (1988) [Opt. Spectrosc. **65**, 307 (1988)].

[20] A. L. Zagrebin and S. I. Tserkovnyi, Opt. Spektrosk. **75**, 276 (1993) [Opt. Spectrosc. **75**, 161 (1993)].

[21] M. H. Alexander, T. Orlikowski, and J. E. Straub, Phys. Rev. A **28**, 73 (1983).

[22] B. Pouilly and M. H. Alexander, J. Chem. Phys. **86**, 4790 (1987).

[23] M. H. Alexander and B. Poully, J. Chem. Phys. **90**, 5373 (1990).

[24] B. Pouilly, J. M. Robbe, and M. H. Alexander, J. Chem. Phys. **91**, 1658 (1989).

[25] B. Pouilly and M. H. Alexander, Chem. Phys. **145**, 191 (1990).

[26] T. Duho and B. Pouilly, J. Chem. Phys. **101**, 7554 (1994).

[27] C. J. Smith, J. P. Driessen, L. Eno, and S. R. Leone, J. Chem. Phys. **96**, 8212 (1992).

[28] E. Czuchaj, F. Rebentrost, H. Stoll, and H. Preuss, Chem. Phys. **138**, 303 (1989).

[29] E. Czuchaj, F. Rebentrost, H. Stoll, and H. Preuss, Chem. Phys. Lett. **182**, 303 (1991).

[30] W. Behmenburg, A. Makonnen, A. Kaiser, F. Rebentrost, V. Staemmler, M. Jungen, G. Peach, A. Devdariani, S. I. Tserkovnyi, A. L. Zagrebin, and E. Czuchaj, J. Phys. B **29**, 3891 (1996).

[31] F. Masnou-Seeuws, J. Phys. B **15**, 884 (1982).

[32] M. H. Alexander, J. Chem. Phys. **96**, 6672 (1989).

[33] B. Pouilly, J. Chem. Phys. **95**, 5861 (1991).

[34] D. A. Varshlovich, A. N. Moskalev, and V. Khersonskii, *Quantum Theory of Angular Momentum* (World Scientific, Singapore, 1988).

[35] E. I. Dashevskaya and E. E. Nikitin, J. Chem. Soc., Faraday Trans. **89**, 1567 (1993).

[36] A. Berengolts, E. I. Dashevskaya, and E. E. Nikitin, J. Phys. B **26**, 3847 (1993).

[37] A. Berengolts, E. I. Dashevskaya, E. E. Nikitin, and J. Troe, Chem. Phys. **195**, 271 (1995).

[38] E. E. Nikitin, in *Atomic, Molecular and Optical Physics Handbook*, edited by G. W. F. Drake (AIP New York, 1996), p. 561.

[39] E. E. Nikitin and K. Taulbjerg, J. Phys. B **27**, 2259 (1994).